The trichothecene mycotoxin deoxynivalenol facilitates cell-to-cell invasion during wheat-tissue colonisation by *Fusarium graminearum*

Victoria Armer[1, 2], Martin Urban[1],Tom Ashfield[3], Michael J. Deeks[2] * and Kim E. Hammond-Kosack[1] *

1. Protecting Crops and the Environment, Rothamsted Research, Harpenden, AL5 2JQ, UK.
2. Biosciences, Geoffrey Pope Building, University of Exeter, Stocker Road, Exeter, EX4 4QD, UK.
3. Crop Health and Protection (CHAP), Rothamsted Research, Harpenden, AL5 2JQ, UK.

*Corresponding authors email addresses: m.deeks@exter.ac.uk; kim.hammond-kosack@rothamsted.ac.uk

Abstract

Fusarium Head Blight (FHB) disease on small grain cereals is primarily caused by the ascomycete fungal pathogen *Fusarium graminearum*. Infection of floral spike tissues is characterised by the biosynthesis and secretion of potent trichothecene mycotoxins, of which deoxynivalenol (DON) is widely reported due to its negative impacts on grain quality and consumer safety. The *TRI5* gene encodes an essential enzyme in the DON biosynthesis pathway and the single gene deletion mutant, *ΔTri5*, is widely reported to restrict disease progression to the inoculated spikelet. In this study, we present novel bioimaging evidence revealing that DON facilitates the traversal of the cell wall through plasmodesmata, a process essential for successful colonisation of host tissue. Chemical complementation of *ΔTri5* did not restore macro- or microscopic phenotypes, indicating that DON secretion is tightly regulated both spatially and temporally. A comparative qualitative and quantitative ultrastructural cellular morphology analysis revealed infections had no impact on cell wall thickness. Immuno-labelling of callose at plasmodesmata during infection indicates that DON can increase deposits when applied exogenously, but is reduced when *F. graminearum* hyphae are present. This study highlights the complexity of the inter-connected roles of mycotoxin production, cell wall architecture and plasmodesmata in this highly specialised interaction.

Introduction

Fusarium graminearum (teleomorph *Gibberella zeae*) is an ascomycete fungal pathogen and the main causative agent of Fusarium Head Blight (FHB), or scab disease, on wheat. *F. graminearum* infects wheat floral tissues at flowering (anthesis), secreting many cell wall-degrading enzymes (CWDEs), other proteins and metabolites as well as mycotoxins that contaminate the developing grain, rendering it unsuitable for both human and livestock consumption [1]. Among these mycotoxins, the sesquiterpenoid type B toxins of the trichothecene class are particularly potent and include deoxynivalenol (DON), nivalenol (NIV), zearalenone (ZEA), and T-2 toxin [2], all of which target the ribosome and inhibit protein synthesis [3]. Trichothecene contamination of grain causes significant economic losses annually [4], destroying wheat crops weeks before harvest and subsequently proliferating during ineffective grain storage/shipment. Epidemics of FHB occur when warm, wet weather coincides with anthesis and are particularly prominent in the mid-West USA, Asia, Brazil and Northern Europe [4, 5]. Novel genetic targets are required to help control outbreaks of FHB due to the prevalence of resistance to the major class of azole fungicides in global *F. graminearum* strains [6]. Incidences of FHB outbreaks are expected to increase as climate change increases precipitation around wheat harvests [5]. Hence, it is imperative that the infection biology of *F. graminearum* is explored further to aid in the development of resistant wheat varieties and precise chemical control, with the overall aim of minimising FHB-associated reductions in cereal yields and to improve human/animal health.

The infection cycle of FHB commences with the dispersal of conidia (asexual) or ascospores (sexual) by rain droplet-induced splashes or wind onto wheat plants. During a typical infection of wheat at crop anthesis, germinating spores enter the host floral tissues through natural openings, such as stomata [7] and cracked open anther sacs, or have been reported to form penetration pegs on the abaxial surface of the palea and lemma tissues of the wheat spikelet [8]. Host-tissue colonisation continues with the invasive hyphae growing both intercellularly and intracellularly. *F. graminearum* has been noted to have a 'biphasic' lifestyle, whereby the advancing infection front is split between macroscopically symptomatic and symptomless phases [9]. The symptomless phase is hallmarked by apoplastic growth, and the symptomatic by extensive intracellular growth. What initiates this switch is not yet known and is a subject of great interest. During later stages of infection, *F. graminearum* secretes CWDEs in great abundance [10] to facilitate infection by deconstructing wheat cell walls. At the rachis internode, invasive hyphae have been reported to enter vascular elements [8] and grow through the remaining wheat spike within the vasculature as well as in the cortical tissue surrounding the vascular bundles. Furthermore, within the chlorenchyma band of the rachis, *F. graminearum* produces perithecia, sexual reproductive structures, completing its lifecycle [11]. Post-harvest, *F. graminearum* overwinters saprophytically on crop debris or within the soil, thereby infecting subsequent crop cycles. The presence of *F. graminearum* in the soil can be the primary cause of seedling blight and root rot in subsequent wheat crops [12].

Intracellular growth by *F. graminearum* has been previously reported to utilise plasmodesmata (PD) [13, 14]. PD are cytoplasmic communication channels that symplastically bridge the cell walls by an appressed endoplasmic reticulum (ER), known as a desmotubule, within a plasma membrane (PM) continuum stabilised by proteins connected to both the ER and PM [15]. PD are instrumental to cellular signalling, allowing for the transport of sugars, ions and small proteins, to

name a few. However, plants can adjust the permeability of PD by the deposition of callose, mediated by the action of callose synthases and β-1,3-glucanases [16] at PD junctions. This callose plugging leads to the symplastic isolation of cells that are damaged or under pathogen attack thereby restricting the movement of secreted pathogen effector proteins, toxins and other metabolites. PD have a major role in host plant defence against viruses, bacteria and fungi [16]. *F. graminearum* exploits the plasmodesmatal transit highways by excreting β-1,3-glucanases: enzymes that catalyse the breakdown of the 1,3-O-glycosidic bond between glucose molecules in callose. RNA-seq analysis of *F. graminearum* infection of wheat spikes found that several Fusarium β-1,3-glucanases are upregulated in the host plant from as early as 6 hours post-infection and peaking between 36-48 hours after inoculation [17].

The trichothecene mycotoxin DON is a well-reported virulence factor in wheat floral tissues and biosynthesis of the toxin requires the *TRI5* gene, encoding the enzyme trichothecene synthase [18]. Deletion of the *TRI5* eliminates the ability of *F. graminearum* to synthesise DON [19], and infection of wheat floral tissues by the single gene deletion mutant (*ΔTri5*) is restricted to the inoculated spikelet, and results in the production of eye-shaped lesions on the outer glume [13, 20]. Conversely, expression of *TRI5* in wild-type *F. graminearum* is correlated with DON accumulation *in planta* [21]. In non-host pathosystems, such as the model plant species *Arabidopsis thaliana*, infection of floral tissues with the single gene deletion mutant *ΔTri5* causes a wild-type disease phenotype, indicating that DON is not a virulence factor in this interaction [20]. Additionally, *ΔTri5* has been demonstrated to produce wild-type disease symptoms in wheat coleoptiles [19], indicating that DON has a specific and targeted role during infection of the wheat floral tissues. Through the use of fluorescent marker reporter strains, the *TRI5* gene has been shown to be induced during infection structure formation on wheat palea [22]. However, the absence of *TRI5* in a *F. graminearum ΔTri5-GFP* strain did not impact the ability of *F. graminearum* to form infection cushions during initial time points of infection [22].The DON mycotoxin naturally occurs as two chemotypes, 15-ADON and 3-ADON, and individual *F. graminearum* strains secrete either toxin type. The wild-type (WT) strain used in this study, PH-1, synthesises 15-ADON. Host-plant resistance to DON is a characteristic of type II FHB resistance, whereby fungal advancement does not proceed beyond the rachis node [23].

Whilst the macro-biology and some aspects of the cellular biology of the single-gene deletion mutant *ΔTri5* have been previously studied, the mode of restriction of *ΔTri5* remains to be elucidated. Postulations have been made around the role of DON during host-tissue colonisation, specifically relating to the targeting of ribosomes and the subsequent, broad-spectrum, protein translation inhibition [24]. However, what host defence mechanisms are targeted/specifically affected by DON have not been explored *in planta*. This study aims to re-evaluate the infection biology of the *ΔTri5* strain, and hence the role(s) of DON, during host-tissue colonisation through a combination of molecular and microscopy techniques. Through qualitative and quantitative image analysis of wheat floral tissues during WT and *ΔTri5* infection, we report that the *ΔTri5* single gene deletion mutant has an impaired ability to traverse plasmodesmata. We also find no evidence to support the hypothesis that a general increase in plant cell wall thickening occurs in the absence of DON production, whereby the upregulation of cell wall defences occurs during pathogen attack. From the data gathered, we infer that the secretion of DON during host-tissue colonisation is highly specific spatially and temporally. This is indicated by the lack of increase in virulence in the *ΔTri5* mutant when supplied with DON at the point of inoculation in our study. In light of these

discoveries, we pose new questions surrounding *F. graminearum* infection biology, cell wall colonisation and wheat host defence mechanisms.

Results

The role of DON during *F. graminearum* infection of wheat floral tissues was addressed through a multifaceted approach. We applied a combination of detailed cell biology, molecular and ultrastructural morphology analyses of floral and coleoptile infections to analyse the effect of DON on hyphae traversing cell walls at PD and the occurrence of the defence response, callose deposition, at plasmodesmata during infections cause by either the WT strain or the single gene deletion mutant *ΔTri5 F. graminearum* strain.

DON is not required for virulence on wheat coleoptiles and chemical complementation does not restore the WT phenotype on wheat spikes

To determine whether DON is not required for virulence on wheat coleoptiles under our conditions the fully susceptible cv. Apogee was tested. Inoculation of wheat coleoptiles revealed no differences in lesion length between the WT PH-1 strain and single gene deletion mutant *ΔTri5* (Fig. 1 (a) and 1(b)). However, RT-qPCR showed that the WT strain did express TRI5 during coleoptile infection, but expression was found to be variable (Fig. 1 (c)) This finding supports a previous study by Qui et al. (2019), who reported accumulation of transcripts of another TRI gene, *TRI4*, also required for trichothecene mycotoxin biosynthesis.

Next, we asked whether the same host and pathogen genotypes showed different DON dependencies during floral tissue interactions. Disease progression of WT, *ΔTri5* and DON-complemented strains were analysed by tracking visible disease symptom development on the outer glume and rachis of inoculated wheat spikes. The single *ΔTri5* mutant was restricted to the inoculated spikelet in all instances. Chemical complementation of the *ΔTri5* mutant with DON (35ppm) applied along with the conidia failed to restore the macroscopic WT spikelet phenotype occurring on the inoculated spikelet or spikelet-to-spikelet symptom development. DON concentration was not detrimental to either spore germination or early spore germling growth (Supplementary file S1). Interestingly, co-inoculation of WT *F. graminearum* with DON at the same concentration did not result in any observable advancement of disease symptoms (Fig. 2 (a)). Application of DON (35ppm) alone did not induce any macroscopic disease symptoms and visually equated to the water only (dH_2O) mock-inoculated samples (Fig. 2 (d), 3(a)). The area under the disease progression curve (AUDPC) analysis revealed that the PH-1 and PH-1 + DON supplementation floral infections had significantly greater disease progression than the *ΔTri5*, *ΔTri5* + DON, DON only, and mock-inoculated treatments (Kruskal-Wallis, $p=2.8e^{-10}$; Fig. 2 (b)). To quantify the levels of DON present in all treatments at the end of disease progression (day 14), a DON-ELISA test was carried out to determine final 15-ADON concentrations. PH-1 and PH-1 + DON samples had an average DON concentration of over 30 ppm, whilst all other treatments had no detectable (<0.5ppm) DON (Fig. 2 (c)). This indicates that the addition of DON to WT inoculum did not stimulate further DON production and confirms that the PH-1 *ΔTri5* mutant is impaired in DON biosynthesis. Of note, the lack of detection of DON in the *ΔTri5* + DON and DON alone samples is likely due to the detoxification of DON by wheat plants to DON-3-glucoside, the latter is undetectable by the competitive enzyme-labelled immunoassay kit used in this study. The conjugation of DON to DON-3-glucoside, catalysed by a UDP-glucosyltransferase, *in planta* is difficult to detect through its

increased molecule polarity and is thus known as a 'masked mycotoxin' [25]. A visual representation of disease progression occurring in each treatment is shown in Fig. 2 (d).

Previously, a qualitative difference in the appearance of macroscopic disease symptoms on the glumes between the WT and the *ΔTri5* mutant has been demonstrated [20]. In this study, we have extended this observation and explored the macroscopic as well as the microscopic disease symptoms. Macroscopically, we were able to confirm the *ΔTri5*-inoculated spikelets exhibited 'eye-shaped' lesions on the outer surface of the glume by 7dpi (Fig. 3 (a)). These differed from the characteristic fawn brown 'bleaching' of the spikelet tissues observed in the WT interaction at 7dpi (Fig. 3 (a)). Chemical complementation of *ΔTri5* did not restore the WT phenotype nor visibly increase the severity of the WT disease phenotype. To quantify the diseased area, inoculated spikelets were imaged at 5 and 7dpi and analysed using the Lemnagrid software for diseased area. The PH-1 and PH-1 + DON spikelets had a greater area exhibiting disease symptoms than both the *ΔTri5* and *ΔTri5* + DON treatments (Fig. 3 (b)). N. B. Computational restrictions in spikelet parsing from background led to minor, insignificant disease symptoms for DON and mock samples.

The *ΔTri5* mutant is inhibited in its ability to traverse plasmodesmata during host-tissue colonisation

Resin-embedded samples of the lemma, palea and rachis spikelet components revealed changes in ultrastructural cellular morphology at different points of infection (Fig. 4). In the palea and lemma parenchyma tissue layer, the *ΔTri5* and *ΔTri5* + DON infected samples exhibited extensive cell wall degradation and colonisation by invasive hyphae (Fig. 5), similarly to the WT infection. However, in the adaxial layer of the palea and lemma tissues, the hyphae in the *ΔTri5* and *ΔTri5* + DON samples rarely penetrated into the thicker-walled cells (Fig. 5(a)-(d)). Mirroring the macroscopic lack of symptoms in the rachis, the *ΔTri5* rachis samples never contained invasive hyphae at either 5 or 7 dpi (Fig. 5(e)). In the PH-1 and PH-1 + DON infected samples, invasive hyphae proliferated throughout the entirety of the lemma, palea and rachis tissues, causing extensive cell wall degradation (Fig. 4). To penetrate the adaxial layer, the PH-1 hyphae utilised cell wall pits resembling PD pit fields (Fig. 4(c)). In these instances, the hyphae constricted considerably to traverse the cell wall. Traversing of the cell wall through PD pit fields was not observed in *ΔTri5* and *ΔTri5* + DON samples at either time point (Fig. 5). In general, where hyphae had invaded cells, the cell contents, notably nuclei, chloroplasts and evidence of cytoplasm, were not observed, indicating cell death. In the palea and lemma tissues of the PH-1 infected samples at 7dpi, evidence of 'ghost' hyphae was identified. These are characterised by a lack of cellular contents [9] and indicate autophagy in older infection structures as the infection front advances into the host plant.

To aid elucidation of the role of DON during infection of wheat floral tissues, cell wall thickness from resin-embedded wheat samples was measured along the adaxial layer of lemma and palea tissues, and in the visibly reinforced regions of rachis tissue, for all treatments. In the adaxial layer of the lemma, palea and rachis tissues, cell wall thickness was found not to differ between treatments, particularly between those with and without the presence of DON (Fig. 6). This unanticipated result indicates that cell wall reinforcements are not evident at this level of resolution, and are not impacted by the presence of DON. However, it is worth noting that extensive cell wall degradation was present in the abaxial layer of palea and lemma tissues. This microscopic phenotype was not quantified but is most likely caused by the release of CWDEs from *F. graminearum* hyphae (Fig. 6).

In order to gain a thorough understanding of infection, a scanning electron microscopy analysis was used. SEM micrographs of rachis post spikelet inoculation with WT PH-1 at 5dpi revealed several notable interactions, including intracellular growth through cells still containing cytoplasm, apoplastic growth between cells, hyphal constriction and cell wall traversing and gaps in rachis cell walls (Fig. 7(a), (b) and (d)). Micrographs of *ΔTri5*-infected lemma tissue at 5dpi confirmed the resin analysis, whereby extensive cell wall degradation is observed in the parenchyma tissue layer (Fig. 7(c)).

Immuno-labelling of callose during infection reveals reduced deposits in the WT infection and phloroglucinol staining indicates lignin-based defence response(s)

Resin sections of PH-1, *ΔTri5* and mock-inoculated wheat floral tissues were analysed for the presence of callose at junctions in the cell wall (Fig. 8 and Fig. 9). Immuno-labelling for the presence of callose confirmed the material of pit structures was consistent with plasmodesmata. Imaging revealed that in both WT (PH-1) and DON-deficient (*ΔTri5*) *F. graminearum*-inoculated spikes there was an increased frequency of instances where callose was deposited at plasmodesmatal junctions compared to mock-inoculated controls (Fig. 9). However, the DON only inoculated samples exhibited a marked increase in callose in both lemma and rachis tissues, indicating that callose deposition had been induced in a manner consistent with a basal immune response to symplastically isolate cells after the detection of the DON toxin.

Spikelets of wheat inoculated with WT PH-1 and *ΔTri5* were sampled at 5dpi for analysis of the lignin response. This investigation was prompted by the presence of localised 'eye-shaped' lesions in the *ΔTri5*-infected samples. Darker staining by the phloroglucinol indicates a higher lignin content, which was found to be most notable in the *ΔTri5*-infected lemma tissue (Fig. 10). This was surprising, as the lesions are present on the glume. Whilst this was not quantified, the WT PH-1 and mock-inoculated controls are visually comparable, indicating that WT *F. graminearum* may have a role in dampening pathogen-induced lignin upregulations, possibly through the action of DON. This proposes the hypotheses that in the absence of trichothecene mycotoxins, wheat is able to upregulate lignin defence pathways.

Discussion

This study has re-examined and extended knowledge on the restricted host tissue colonisation phenotype previously reported in wheat spikes for the non-DON-producing *ΔTri5* single gene deletion mutants of *F. graminearum*. The study was catalysed by the lack of published cellular information available on how DON, produced by the advancing *F. graminearum* hyphae, actually facilitates the extraordinary effective and speedy disease progression consistently observed in the spikes of susceptible wheat cultivars. DON has long been classified as a key virulence factor in the *F. graminearum*-wheat interaction [18, 19, 13]. DON facilitates the host-tissue colonisation of the rachis and is essential for successful internal spikelet-to-spikelet growth of hyphae through the entire floral spike. However, prior to this study, the morphological and cellular responses underlying this macroscopically well documented phenomenon had not been explored. In this study our two primary aims were (a) to identify the morphological differences in the hyphal infection routes between the wildtype (WT) and *ΔTri5* strains during wheat floral infections, and (b) to focus on the

248 roles of plasmodesmata and cell wall thickness and content during hyphal colonisation due to their
249 potential to delay, minimise or cease fungal progression through the numerous internal complexities
250 that the wheat spike architecture presents to the Fusarium hyphae.

251 As described above, our experimentation confirmed that the *ΔTri5* mutant could sufficiently
252 colonise the lemma and palea tissues but not the rachis [13, 20]. Similarly, our results concurred
253 with results that the DON-deficient *F. graminearum* strain could not grow beyond the rachis node
254 due to the presence of inherently thicker cell walls [13]. However, our quantitative comparative
255 analysis of WT and DON-deficient interactions revealed no differences between cell wall thickness at
256 two timepoints, or with the control mock inoculated tissues, indicating that cell walls do not increase
257 in thickness *per se* as part of a locally occurring defence response. Upon further microscopic analysis
258 in the current study, the main reason for hyphal arrest in the rachis node was revealed. The DON-
259 deficient *ΔTri5* mutant could not enter wheat cells with inherently thicker cell walls because the
260 hyphae could not pass through plasmodesmata. This phenomenon was frequently observed in both
261 the cortical and sclerenchyma cell layers. As a result, the *ΔTri5* hyphae accumulated within and
262 between the neighbouring thinner-walled parenchyma cells. Presumably, in these thicker-walled
263 tissue layers, in the absence of DON the genome-predicted arsenal of *F. graminearum* CWDEs are
264 less effective at the advancing hyphae front in deconstructing the cell wall matrix. Alternatively,
265 other so far uncharacterised secreted proteinaceous effectors fail to correctly manipulate these
266 potential gateways into the neighbouring wheat cells in the absence of DON. The analysis of resin
267 sections revealed that cell walls within the adaxial layer of lemma and palea tissues were not thicker
268 in infected samples. Although this rules out additional cell wall reinforcements, these findings do not
269 eliminate cell wall compositional changes. Our results indicate that lignin content increases in the
270 lemma tissue, which strengthens the tissue and hence emphasises the role of plasmodesmata as cell
271 wall portals in host-tissue colonisation. Our SEM inquiry of the infected tissues indicates that
272 plasmodesmata, when used by the advancing hyphal front, are potentially 'dead portals', that lack
273 the desmotubule symplastic bridge between neighbouring cells. This would therefore suggest that
274 plasmodesmatal defences, namely callose deposition, are eliminated prior to hyphal constriction and
275 traversing of the cell wall. However, other microscopy techniques will need to be used to explore
276 whether desmotubule connections are consistently present or absent at the point of hyphal
277 traverse. Collectively, these data suggest that the broad-spectrum consequences of DON targeting
278 could prevent the synthesis and action of key defence enzymes at plasmodesmata. This could be
279 explored by a combined comparative proteomics, phosphoproteomics and RNAseq analysis of the
280 WT and *ΔTri5*-infections to elucidate the wheat defence responses occurring at the advancing
281 *Fusarium* hyphal front that are reduced and/or eliminated by the presence of DON.

282 The deposition of callose at the plasmodesmatal junction by callose synthases has been
283 demonstrated to be induced by various biotic stress-inducing pathogens [26]. The role of callose
284 differs with cellular location: callose polymers are a structural component of papillae in various
285 cereal species that form below appressoria produced by fungal pathogens such as the powdery
286 mildew *Blumeria graminis* f. sp. *hordei*, whereby elevated callose deposition in highly localised
287 papillae in epidermal cells result in resistance to fungal infection [27]. In vascular tissue, callose can
288 be deposited to restrict vascular advancements by wilt pathogens, including by *Fusarium* and
289 *Verticillium* species [28]. To investigate the potential of DON impacting upon plasmodesmatal
290 occlusion following our discovery of the impeded traversal of plasmodesmata by the *ΔTri5* strain, we
291 immuno-labelled callose in resin-embedded sections of wheat floral tissues. We found that DON

strongly induced callose depositions, and callose deposition was also moderately increased in WT and *ΔTri5* infected lemma and palea tissues. This indicates that callose deposition is upregulated as a defence response when DON is present. However, in the WT infection, we observed a frequency of callose depositions similar to the non-DON producing *ΔTri5* strain indicating an interruption or targeted degradation of callose occlusions by *F. graminearum* invasive hyphae. The secretion of glycoside hydrolase (GH) proteins that break down □-1,3-glucans such as callose have not been explored with respect to the *Fg*-wheat interaction, although GH12 family proteins that break down xyloglucan in plant cell walls appear to be implicated in virulence [29]. In the *ΔTri5* infections, in the absence of DON other hyphal components and /or secreted molecules may be responsible for the modest callose deposition at the plasmodesmatal junction.

Intracellular colonisation through the rachis node and beyond in the rachis internode possibly requires DON and is therefore required for the second intracellular phase of the biphasic lifestyle described for *F. graminearum,* with extracellular apoplastic growth characterises the initial 'stealth' phase of infection [14]. If this is the case, then lacking the ability to traverse plasmodesmata would restrict direct acquisition of nutrients from host cells by the fungal hyphae. The TRI biosynthetic gene cluster required for DON biosynthesis is transcriptionally activated early during infection, peaking between 72 and 120 hrs post-inoculation [30, 31], when infection is largely restricted to the palea, lemma and glume tissues. TRI biosynthesis is regulated by two transcription factors, TRI6 and TRI10, within the biosynthetic pathway. Of note, DON is not required for full virulence of the developing wheat kernel seed coat [13], in addition to our finding in coleoptiles. It has been identified that trichothecene biosynthesis pathway induction was potentially tissue specific and somewhat restricted to the developing grain kernel and rachis node, suggesting that 'kernel tissue perception' by the *Fusarium* hyphae induce the biosynthesis of trichothecene mycotoxins [32]. This suggestion concurs with the report that the trichothecene biosynthesis genes were not induced during *F. graminearum* infection of wheat coleoptiles [33]. However this 'kernel tissue perception' idea has not been further explored. Gardiner et al. presented evidence that, in addition to their previous reports that exogenous application of amines, such as agmatine, *in vitro* induces TRI5 expression [34], low pH further accelerates expression of the TRI cluster. Other inducers of the DON biosynthetic pathway genes include carbon, nitrogen and light [35]. Other fungal pathogens that are reported to utilise plasmodesmata during infection of cereals include *Magnaporthe orzyae and M. oryzae* pathotype *triticum* which respectively cause rice blast and wheat blast diseases on the floral panicles [36, 37]. Although *Magnaporthe oryzae* does not synthesise trichothecene mycotoxins, the invading hyphae secrete another potent general protein translation inhibitor, namely tenuazonic acid [38]. The effect of this mycotoxin on plasmodesmatal traversing and virulence in *Magnaporthe spp*. has not yet been reported. *F. graminearum* progression into the rachis and through sequential rachis nodes and internodes allows for the successful completion of the disease infection cycle in wheat crops. Typically, perithecia form from the chlorenchyma band of the rachis following prolific hyphal colonisation of this highly specialised photosynthetic tissue layer within the wheat spike [11]. Hence, interruption of WT disease progression prior to this crucial point in the primarily monocyclic infection cycle is of great interest for reducing full virulence of FHB and in particular in reducing the abundance of air dispersed ascospores. Interestingly, infection of barley spikelets with WT *F. graminearum* is solely restricted to the inoculated spikelet, similarly to *ΔTri5* infection of wheat [13]. How this occurs has not yet been explored, but we hypothesise that a lack of transition across plasmodesmata by hyphae may have a role to play in barley rachis node tissue.

Overall, our study indicates that plasmodesmata are the key to successful host-tissue colonisation by *F. graminearum* and that DON, directly or indirectly, facilitates this interaction. We anticipate that the results of this study are considered in future working disease models of the *F. graminearum* - wheat interaction and suggest these incorporate a greater emphasis on tissue and cell wall architecture and composition when considering host susceptibility to fungal pathogens. To this end, we have proposed a new working model (Fig. 11), that summarises our findings around the presence of DON during wheat infection and the impact on callose deposition at plasmodesmata.

Materials and Methods

Fungal growth

The *Fusarium graminearum* reference strain PH-1 (NCBI: txid229533) and the DON-deficient single gene deletion mutant *ΔTri5*, with PH-1 parental background [20], were used in this study. Conidia for glycerol stocks were prepared by culturing on Synthetic Nutrient Poor Agar (SNA) plates containing 0.1% KH_2PO_4, 0.1% KNO_3, 0.1% $MgSO_4 \cdot 7H_2O$, 0.05% KCl, 0.02% glucose, 0.02% sucrose and 2% agar. Plates were left to grow for 8 days at room temperature (RT) with constant illumination under near-UV light (Philips TLD 36W/08). TB3 liquid medium (0.3% yeast extract, 0.3% Bacto Peptone and 20% sucrose) was added to plates to stimulate spore production and left for a further 2 days. Conidia were harvested and stored in 15% glycerol at -80°C in 2ml cryotubes (Thermo Fisher Scientific, MA, USA). Conidial suspensions in water to be used for inoculations were prepared by spreading conidia from glycerol stocks onto Potato Dextrose Agar (PDA, Sigma Aldrich, UK) plates, then growth at RT for 2 days, harvesting with dH_2O and spore concentrations measured with the aid of a haemocytometer (Hausser Bright-line, USA). Experiments were conducted under APHA plant licence number 101948/198285/6.

Plant growth

The susceptible dwarf wheat (*Triticum aestivum*) cultivar (cv.) Apogee was used for all wheat experiments. Seeds were sown in Rothamsted Prescription Mix (RPM) soil (Petersfield Growing Mediums, UK) in P15 pots (approx. volume $7cm^3$) and grown in controlled environment facilities at HSE category 2 (Fitotron®, Weiss Gallenkamp, UK), 16hr light: 8hr dark cycle at 22°C and 18°C respectively, 70% relative humidity and illumination at $2.2x10^3$ µmol m^{-3}.

Coleoptile inoculations

For coleoptile inoculations, Apogee grain were left for 2 days at 5°C in water for imbibition before being placed individually onto cotton in a 24-well tissue culture plate (VWR, USA) and left to germinate for 3 days under high humidity conditions (<90% relative humidity) under normal wheat growth conditions. At 3 days post-sowing, approximately 5mm from the tip of each coleoptile was cut to encourage infection. Inoculations occurred through the placement of a cut pipette tip with a filter paper insert soaked with $5x10^5$ spores/ml solution, with dH_2O used as a negative control. The coleoptiles were left in the dark for 3 days to aid infection, after which inoculation tips were subsequently removed, and coleoptiles were left to grow under normal growth conditions for a further 4 days [39]. Disease phenotypes on the coleoptiles were assessed at 7 days post inoculation by imaging lesions on a Leica M205 FA Stereomicroscope (Leica Microsystems, UK). Each

experimental replicate contained 5 biological samples for each treatment (3 mock-inoculated) and the experiment was repeated 3 times.

Floral inoculations

At mid-anthesis, wheat plants were inoculated with 5 x10^5 spores/ml water conidial suspension of PH-1 or *ΔTri5*, conidial suspension supplemented with DON, DON alone or water (dH_2O) control. DON supplementation of inoculum was 35ppm (Sigma-Aldrich, USA). As previously described [40], a 5µl droplet was placed between the palea and the lemma on each side of the 7th true spikelet from the base. Inoculated plants were placed in a high (<90%) humidity for the first 72 hours of infection, with the first 24 hours in darkness. After 72 hours plants were returned to normal growth conditions.

Disease progression

As above, Apogee at mid-anthesis was inoculated and disease progression was assessed by counting spikelets showing visible symptoms every 2 days after inoculation until 14 dpi. Area Under Disease Progression Curve (AUDPC) [41] was calculated using the 'agricolae' package (version 1.4.0) [42], in R (version 4.0.2). Statistical significance was determined by Kruskal-Wallis one-way analysis of variance through the R package 'ggplot2' (version 3.4.0) [43]

RGB colour classification for disease assessment of dissected spikelets

To quantify disease progression on wheat spikelets at 5 and 7dpi, colour (RGB) spikelets were imaged (iPhone 6s, Apple Inc, US) on both sides with consistent illumination. Diseased area was quantified using a curated programme on the LemnaTec Lemnagrid software (CHAP, York, UK). Diseased area was classified by pixel colour segmentation after application of filters to threshold from the background, identify misclassified pixels and fill in gaps. Area attributed to anthers were omitted from further analysis. The relative area attributed to each classification was then calculated in a custom R script and all samples were normalised to the mean value of 'diseased' of the mock treatment due to background parsing error.

Bioimaging

Inoculated spikelets were dissected from the wheat spikes for internal observations of infected floral tissues. Spikelets were fixed for 24 hr in a solution of 4% paraformaldehyde, 2.5% glutaraldehyde and 0.05M Sorensen's phosphate buffer (NaH_2PO_4: $Na_2HPO_4 \cdot 7H_2O$, pH 7.2), in the presence of Tween 20 (Polyethylene glycol sorbitan monolaurate; Sigma-Aldrich) and subject to a light vacuum for 20s to ensure tissue infiltration. Fixed spikelets were washed 3x with 0.05M Sorensen's phosphate buffer and subsequently underwent an ethanol dehydration protocol at 10% EtOH increments, up to 100% EtOH. Spikelets were dissected into component tissues and embedded with LR White resin (TAAB, Reading, UK) at increasing resin ratios (1:4, 2:3, 3:2, 4:1), followed by polymerisation in the presence of N_2 at 60°C for 16h. Ultra-thin 1µm resin sections were cut from resin blocks using a microtome (Reichert-Jung, Ultracut), placed onto Polysine microscope slides (Agar Scientific, UK) and stained with 0.1% (w/v) Toluidine Blue O in 0.1M Sorensen's phosphate buffer (NaH_2PO_4: $Na_2HPO_4 \cdot 7H_2O$, pH 7.2). Every 10th section was collected for a total of 10 sections per embedded block to fully explore floral tissues and mounted with Permount (Fisher Scientific, UK) prior to imaging on a Zeiss Axioimager 512 (Zeiss, Oberkochen, Germany) at x20 magnification under

brightfield illumination. The experiment was repeated 3 times, with a total of 5 biological replicates for each treatment, with 2 mock samples per batch. In total, 111 resin blocks were explored across a 100um in the centre of the sample, with sections cut every 10µm. Image analysis was conducted in Fiji for ImageJ (version 2.3.0) and statistical analysis was conducted in R (version 4.0.2).

For SEM exploration of floral tissues, spikelets at 5dpi were excised and coated in 50:50 OCT compound (Sakura FineTek) with colloidal graphite (TAAB). SEM analysis was conducted on rachis tissue infected with the WT reference strain PH-1 at 5dpi. Sample preparation occurred in a Quorum Cryo low-pressure system before imaging on a JEOL LV6360 SEM at 5kV with software version 6.04.

Callose immuno-labelling of resin-embedded sectioned material was conducted according as previously described [44]. Briefly, callose was localised by anti-□-1,3-glucan antibodies (Biosupplies, Australia) and secondarily conjugated with rabbit anti-mouse Alexa Fluor 488. Wheat cell walls were counterstained with calcofluor white. Sections were imaged by confocal microscopy on a Leica SP8 confocal microscope, with excitation-emission spectra for AlexFluor-488 at 488nm, 510nm-530nm and 405nm, 450nm-475nm for Calcofluor white. Image analysis for the quantification of callose deposits per cell was conducted in Fiji using maximum projections of Z stacks and channels converted to binary masks. The number of cells in the sample area was calculated using the cell counter tool and callose deposits were counted by the number of discrete Alexa 488-fluorescences between the size of 2 to 12 pixel units to eliminate cross-reactivity with β-1,3-glucans in the fungal cell walls. Callose deposits were quantified in the lemma and rachis tissues only, with 3 biological replicates for each treatment (PH-1, *ΔTri5*, DON, Mock). Further examples are present in supplementary S4 and image analysis methodology is demonstrated in supplementary figure S5.

DON quantification

To determine if the presence of DON in the WT strain inoculum stimulated further DON production, if administered DON could be detected in wheat spike tissues at the end of disease progression (14dpi), and the absence of DON in the *ΔTri5* mutant interaction a competitive enzyme-labelled immunoassay for 15-ADON was employed. Whole wheat spikes after 14 days of disease progression were ground to a fine powder in the presence of liquid nitrogen and 1g of each sample was resuspended in 5ml dH_2O, vortexed until dissolved, incubated in a 30°C water bath for 30 mins and centrifuged for 15 minutes at full speed (13.1g). The supernatant was removed and analysed using the Beacon Analytical Systems Inc Deoxynivalenol (DON) Plate Kit (Cat. 20-0016) according to kit instructions. The OD450 values were measured on a Thermo Varioskan microplate reader (Thermo Scientific, USA). Three technical replicates of each biological replicate (wheat head) were conducted, and the experiment was repeated three times.

Similarly, DON was quantified at 7dpi in WT inoculated coleoptiles. In this instance, the entire coleoptile and seedling from the germinated grain was sampled and followed the same protocol as above.

Expression of the mycotoxin biosynthesis gene TRI5 during coleoptile infection

The trichodiene synthase gene TRI5 was used as a proxy for the relative expression of the trichodiene biosynthesis pathway during coleoptile infection. Total RNA was extracted from whole coleoptiles at 7dpi using the NEB Total RNA extraction kit (NEB) and following kit instructions. First strand cDNA was synthesised using RevertAid First Strand cDNA synthesis kit (ThermoFisherSci) as

per kit instructions and utilising random hexamer primers provided. TRI5 expression was then assessed by qPCR with melt curve using the primers in supplementary S2, with SYBR as the reporter, passive reference as ROX and NFQ-MGB as the quencher. The qPCR with melt curve was conducted in technical and biological triplicate on a QuantStudio™ 6 Pro and results analysed on the complementary Design & Analysis Software v. 2.6.0 (ThermoFisher Scientific, MA, USA). The experiment was conducted 3 times.

Phloroglucinol staining for presence of lignin

A 3% Phloroglucinol (Sigma Aldrich, UK) - HCl solution (Weisner stain) was prepared fresh in accordance with previously described methods [45]. Inoculated wheat spikelets were sampled at 5dpi and cleared in 100% EtOH for 4 days before going through a rehydration series (75%, 50%, 25% and 0% EtOH) at 1 hour per stage. Cleared spikelets were bathed in Weisner stain for 1 hour, or until staining of the tissues becomes evidently saturated. Spikelets were then imaged (OM-D E-M10, Olympus, Japan) under constant illumination and, subsequently, dissected tissues were imaged individually.

Formation of perithecia *in vitro*

Carrot agar was prepared using the method outlined previously [46] and supplemented with DON at 35ppm (w/v) to test for the ability of the WT strain, and the DON trichothecene-deficient deletion mutant, *ΔTri5*, to develop perithecia *in vitro*, for lifecycle completion viability (Supplementary S3). Ability of perithecia to discharge ascospores in the presence of DON was assessed using the same method as described [46].

Statistical analysis

Scripts were written in R (version 4.0.2) for each experimental analysis. Unless otherwise stated, ANOVA followed by Tukey post-hoc test was conducted for parametric datasets and Kruskal-Wallis for non-parametric datasets. The significance threshold was set to $P < 0.05$ in all cases.

Data availability

Publication-related data is available from the corresponding author on request.

Figures

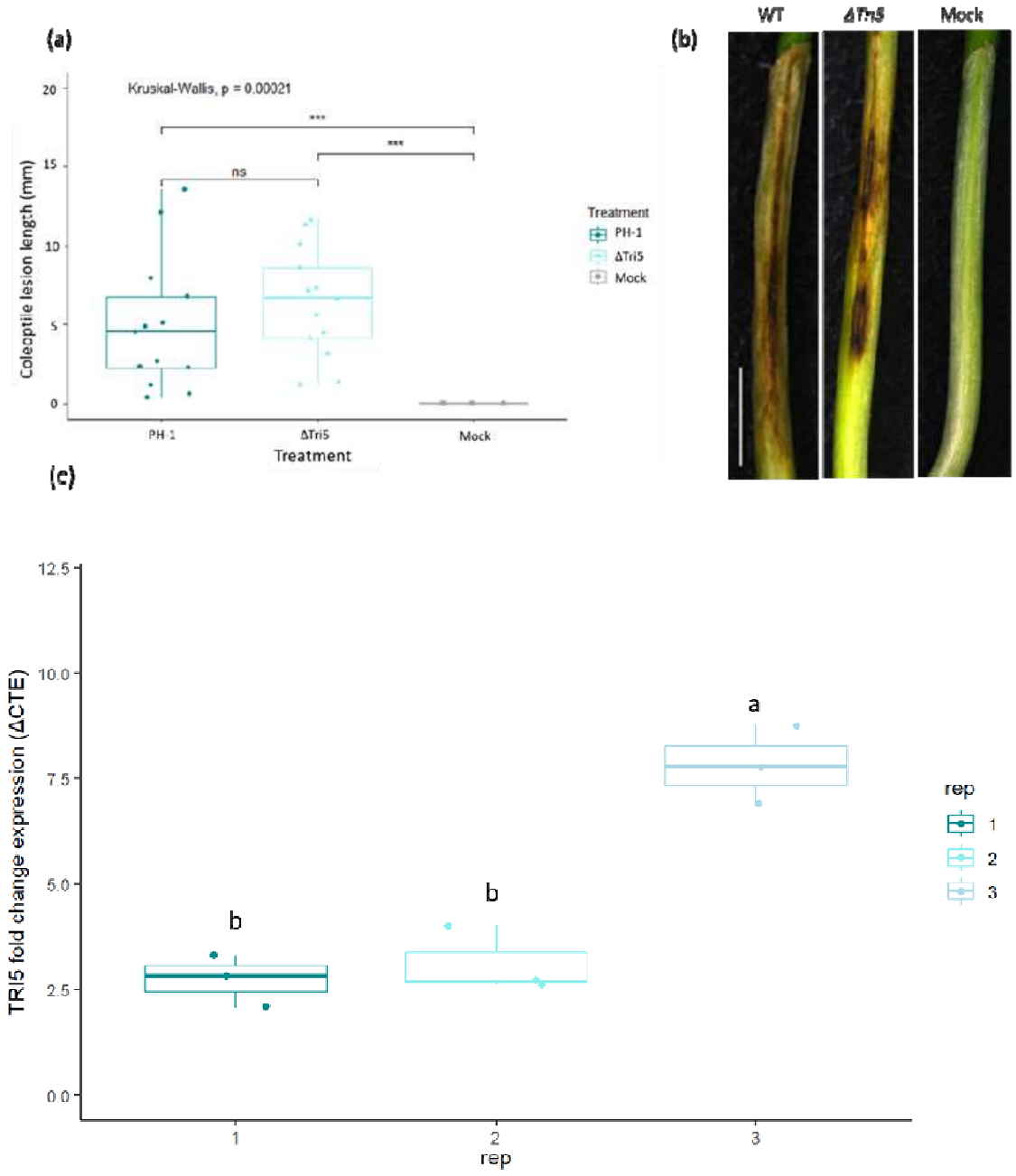

Fig. 1. *F. graminearum* disease formation on wheat coleoptiles (a) Length lesion at 7dpi for PH-1, the *ΔTri5* mutant and mock inoculations, Kruskal-Wallis $p < 0.005$(***). (b) Examples of lesion phenotypes at 7dpi for PH-1, *ΔTri5* and mock inoculations from rep 2, scale bar = 20mm and (c) Relative expression of TRI5 measured using RT-qPCR at 7dpi in wheat coleoptiles, normalised against FgActin and expressed as fold change (ΔCTE). ANOVA, $p < 0.005$ (***), Tukey post-hoc demonstrates group significance.

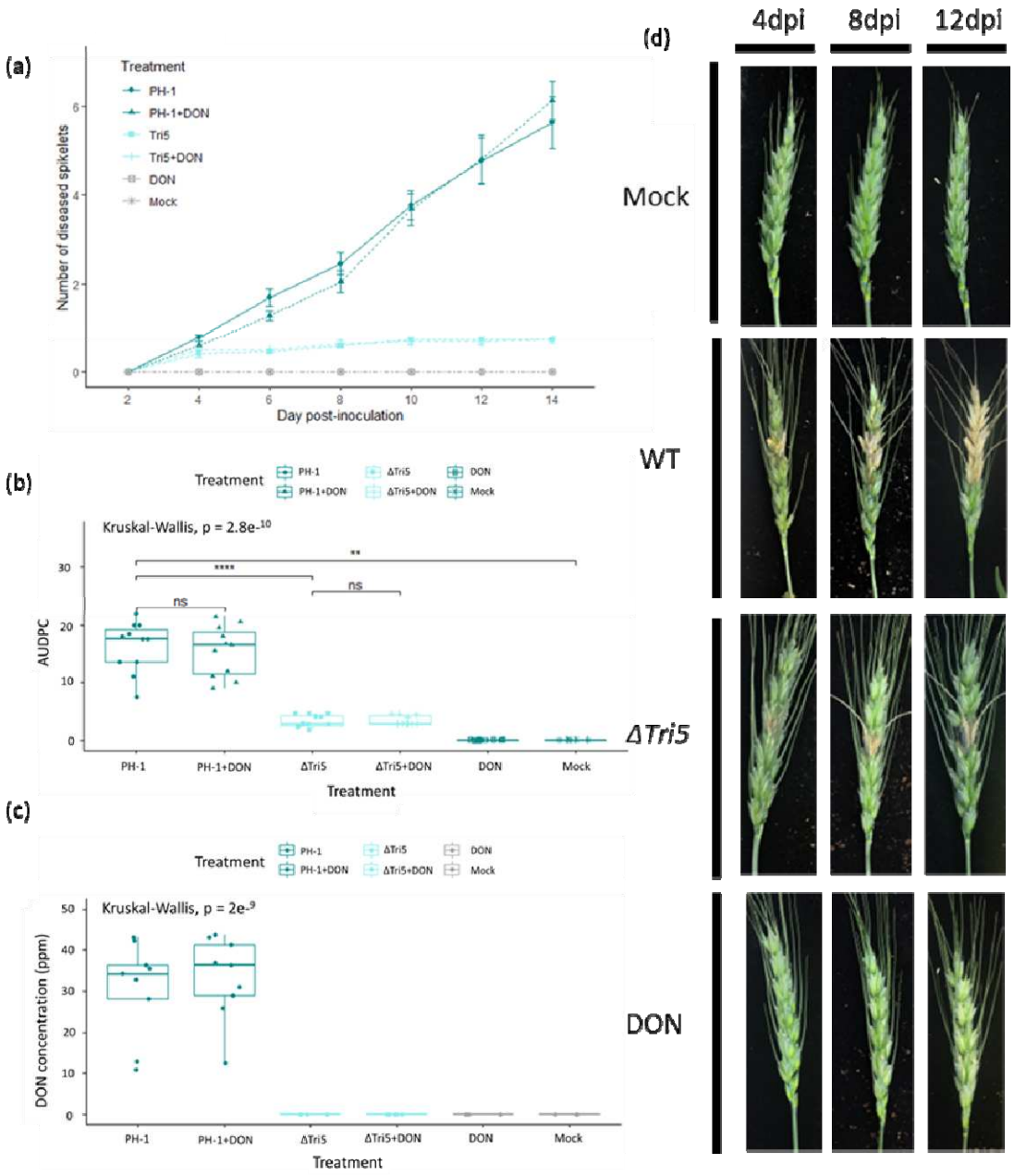

490
491 **Fig. 2. Analysis of whole wheat floral tissues following point inoculations.** (a) Tracked visible
492 disease progression at 2-day intervals to 14 dpi from below the inoculated spikelet. (b) Area Under
493 Disease Progression Curve (AUDPC) for disease progression in panel (a), Kruskal-Wallis p <0.005
494 (***). (c) DON concentrations of wheat spikes at 14 dpi, Kruskal-Wallis p <0.005 (***). (d)
495 Representative disease progression images at selected timepoints of 4, 8 and 12 days.

496

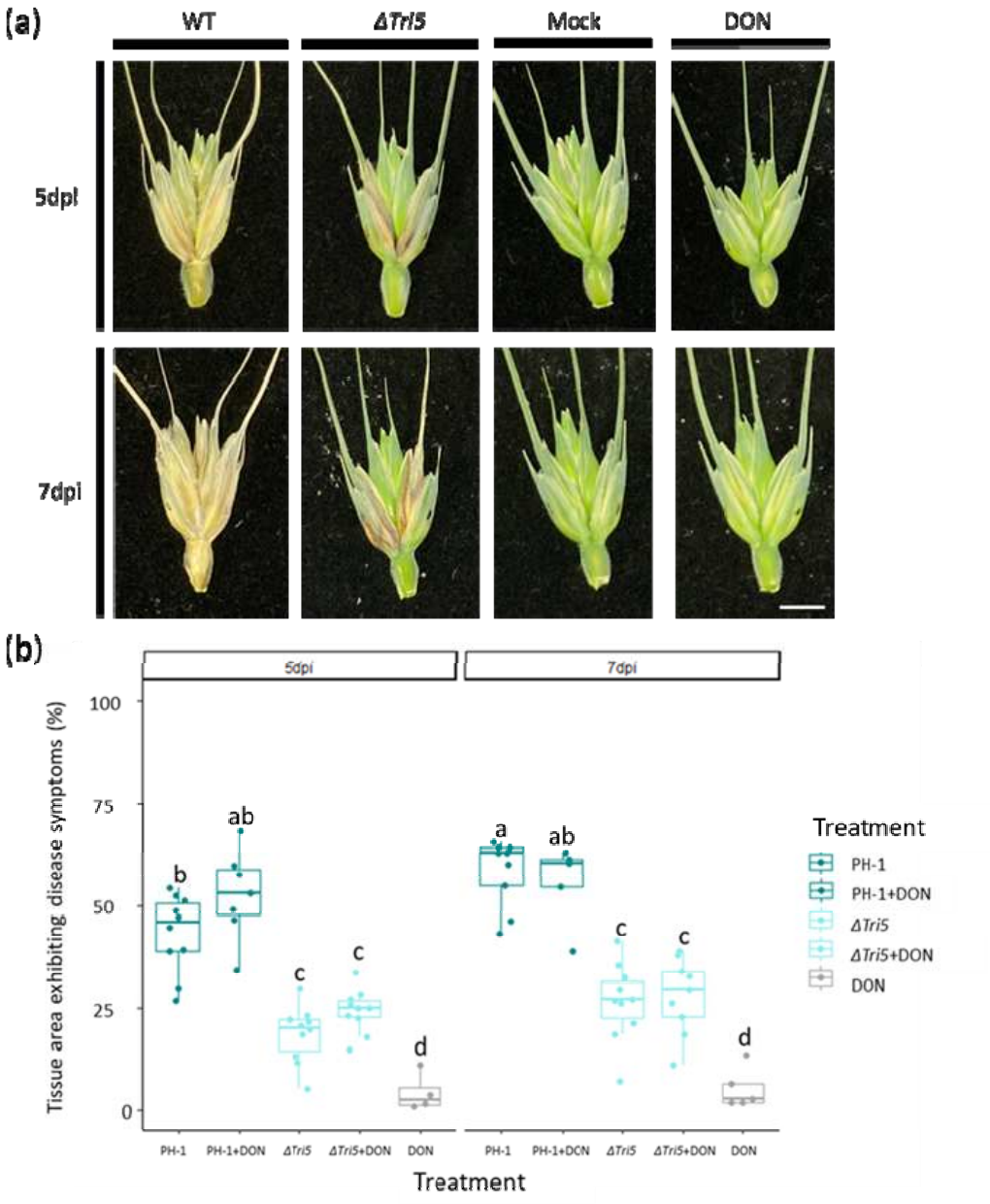

497

498 ***Fig. 3.*** **Quantitative spikelet analysis for disease symptom development.** (a) Examples of dissected
499 spikelets at 5 and 7dpi, scale bar = 10mm. (b) External tissue areas exhibiting disease symptoms at 5
500 and 7dpi as determined by Lemnagrid computational software. ANOVA, $P < 0.005$ (***), Tukey post-
501 hoc denotes group significance.

502

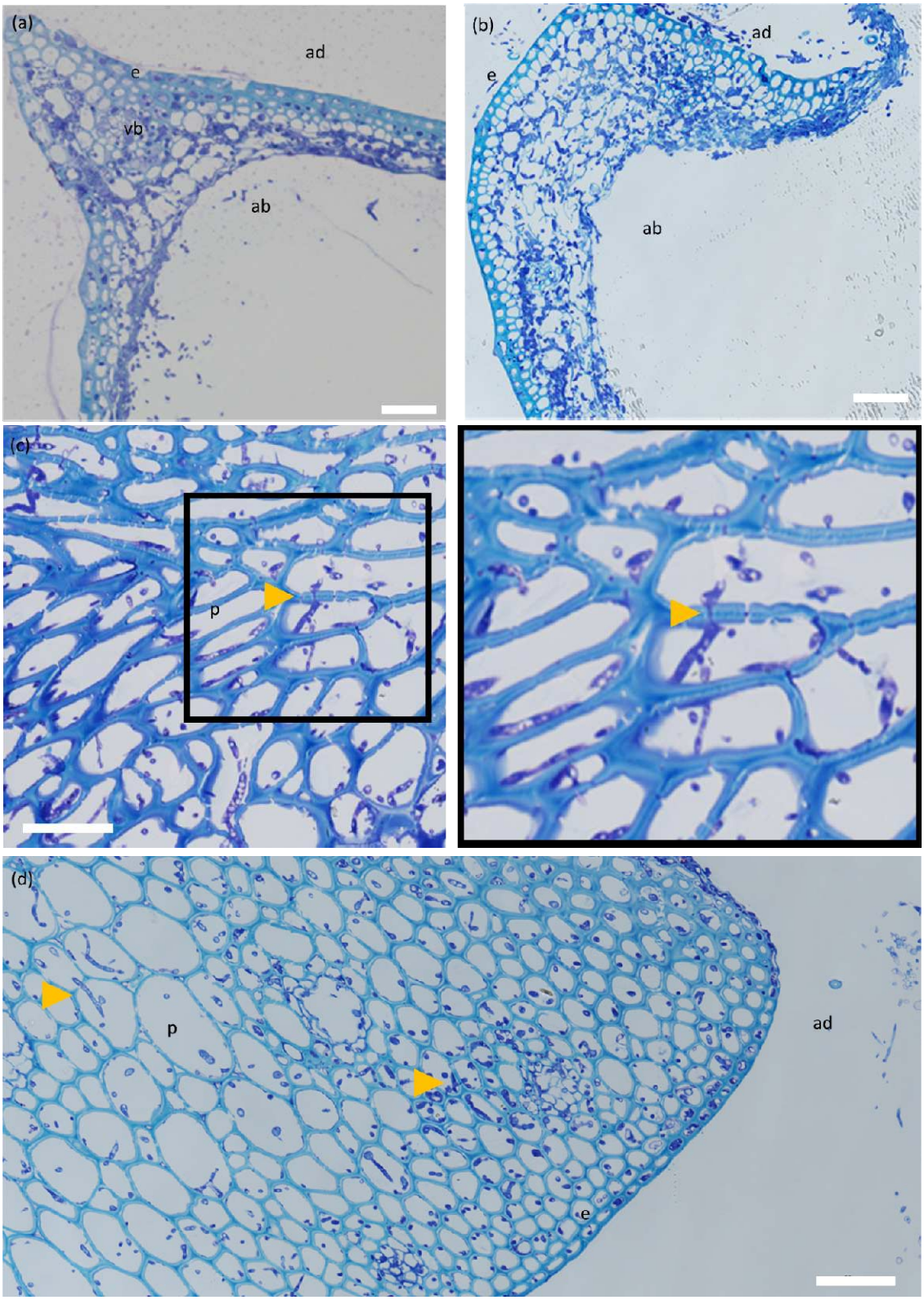

Figure 4. WT-infected wheat floral tissues at 5 and 7 dpi demonstrating aspects of typical infection. (a) Lemma at 5dpi infected with WT *F. graminearum* showing widespread hyphal colonisation throughout the tissue accompanied by hyphal proliferation protruding from the abaxial

layer. (b) A 7dpi WT-infected lemma showing further tissue degradation by cell wall degrading enzymes and considerable hyphal proliferation. (c) Rachis at 5dpi infected with WT *F. graminearum* showing a number of plasmodesmatal crossings by invasive hyphae, indicated by yellow arrowheads, and extensive cell wall degradation of the mesophyll layer by *F. graminearum*- excreted cell wall degrading enzymes. Plasmodesmata can be identified as gaps in the parenchyma layer cell walls, a number of which are indicated by black arrowheads. (d) A 7dpi WT-infected rachis demonstrating durability of parenchyma tissue against cell wall degrading enzymes at later infection timepoints. ab = abaxial layer, ad = adaxial layer, e = epidermal layer, mes = mesophyll, p = parenchyma tissue, vb = vascular bundle. Yellow arrowheads indicate plasmodesmatal crossings by invasive *F. graminearum* hyphae. Scale bar = 50µm.

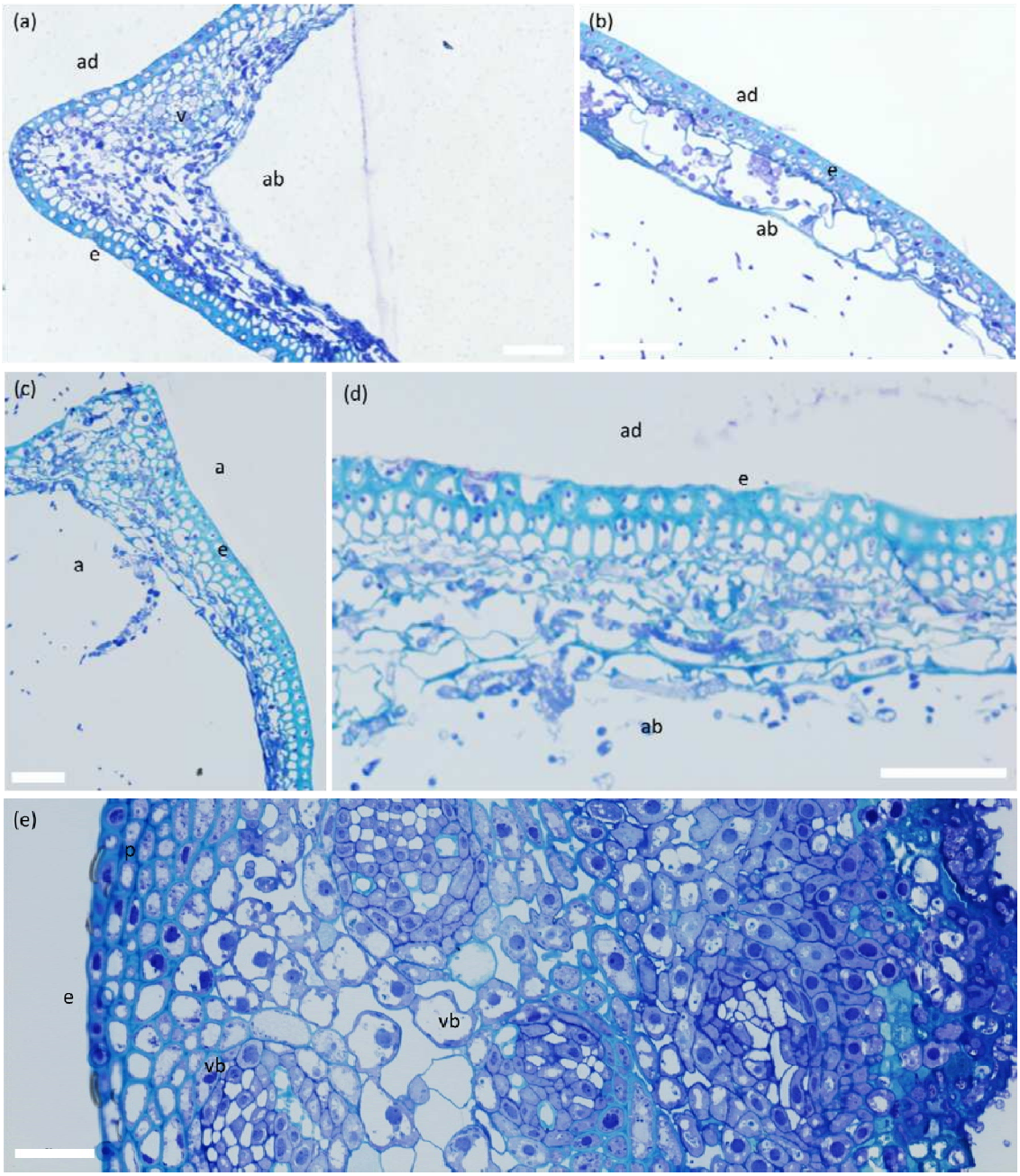

519 **Figure 5. Comparison of *ΔTri5*-infected and *ΔTri5* + DON infected wheat floral tissues at 5 and 7dpi**
520 **showing the similarities and differences between tissue types in various aspects of a typical**
521 **infection.** (a) Lemma at 7dpi infected with *ΔTri5 F. graminearum* with extensive proliferation of
522 invasive hyphae throughout the abaxial layer, but rarely any penetration into the adaxial layer. (b).
523 Palea infected with *ΔTri5* and supplemented with 35ppm DON showing cell wall degradation in the
524 abaxial layer and evidence of external fungal hyphae. (c) Palea at 7dpi infected with *ΔTri5*, with
525 similar symptoms to the lemma at the earlier 5dpi time point. (d) Lemma infected with *ΔTri5* and
526 supplemented with 35ppm DON at 7dpi showing cell wall degradation of the abaxial layer. (e) A
527 rachis section at 5dpi infected with *ΔTri5* and supplemented with 35ppm DON. No evidence of
528 hyphae or cell wall degradation throughout the sample. ab = abaxial layer, ad = adaxial layer, e =
529 epidermal layer, mes = mesophyll layer, p = parenchyma tissue, vb = vascular bundle. No
530 plasmodesmatal crossings by invasive *F. graminearum* hyphae are evident. Scale bar = 50µm.

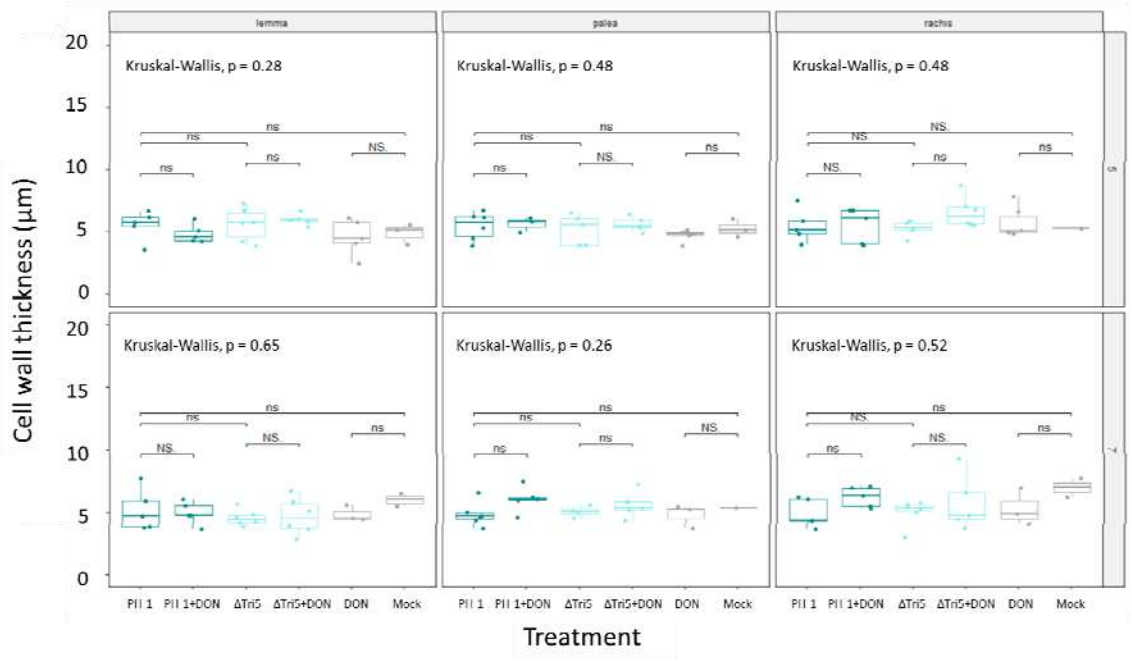

531

532 **Fig. 6. Cell wall thickness of adaxial cell layer in resin samples.** Wheat spikelet tissues of palea,
533 lemma and rachis at 5 and 7dpi time points were analysed, with an average of 10 measurements
534 from a representative resin image of each biological replicate analysed. No significance was
535 determined by Kruskal-Wallis.

536

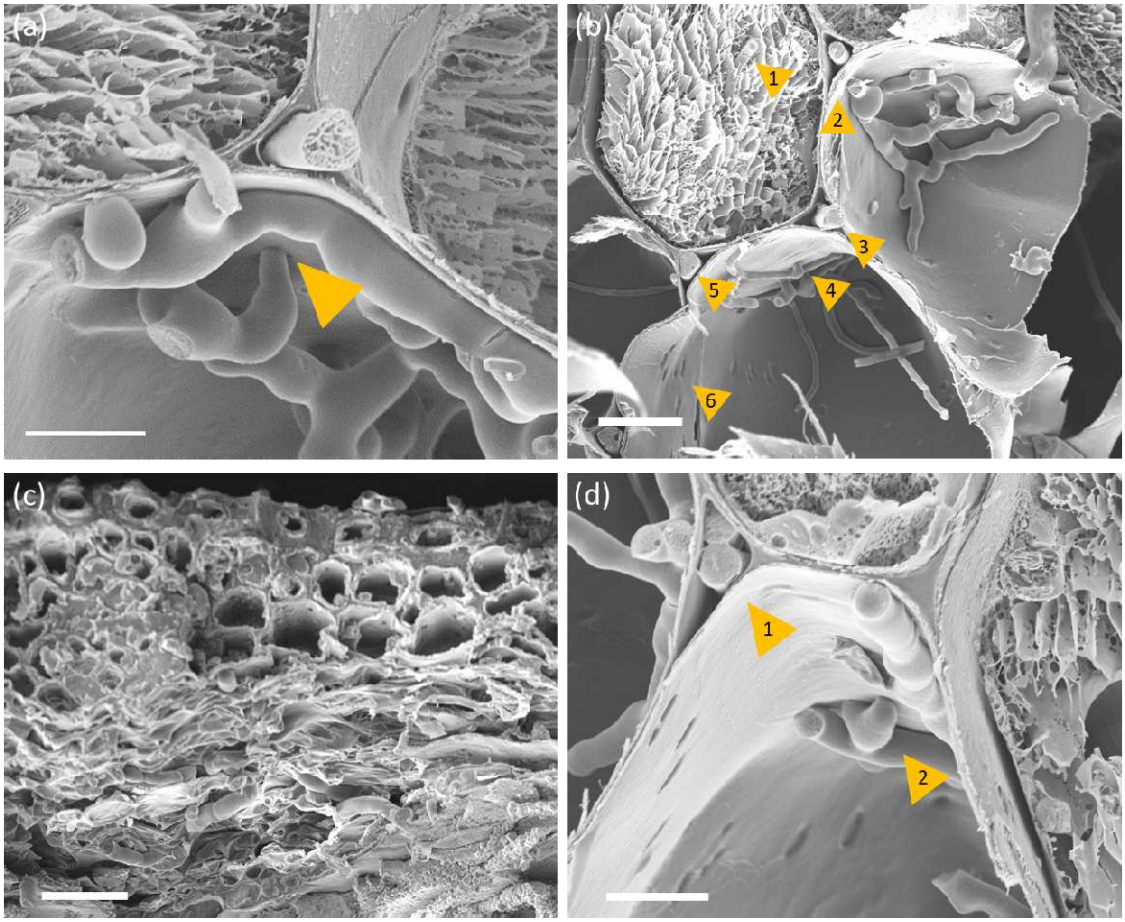

Fig. 7. SEM micrographs of PH-1 and *ΔTri5*- wheat floral interactions. (a) Hypha of the wildtype PH-1 strain crossing through the cell wall at 5dpi in rachis tissue. The numbered yellow arrowhead indicates point of interest. Scale bar = 10μm. (b) Wild-type PH-1 infecting rachis tissue at 5dpi, 1. Intracellular growth in a cell where cytoplasm is still present, 2., 3., and 5. apoplastic growth between cells, 4. Potential crossing of the cell wall by a hypha through a plasmodesma, and 6. 'Holes' in the cell wall that are potential sites of plasmodesmata. Scale bar = 20μm. (c). *ΔTri5*-infected lemma tissue at 5dpi demonstrating extensive colonisation and cell-wall degradation of the parenchyma tissue layer (bottom), but minimal infection in the thicker-walled adaxial layer (top), scale bar = 20μm. (d) Wild-type PH-1 infection of the rachis at 5dpi, 1. Growth of two hyphae through the same apoplastic space in parallel to hyphae growing intracellularly in neighbouring cells to the left and right. 2. Hypha appear to constrict to traverse the cell wall. Scale bar = 10μm.

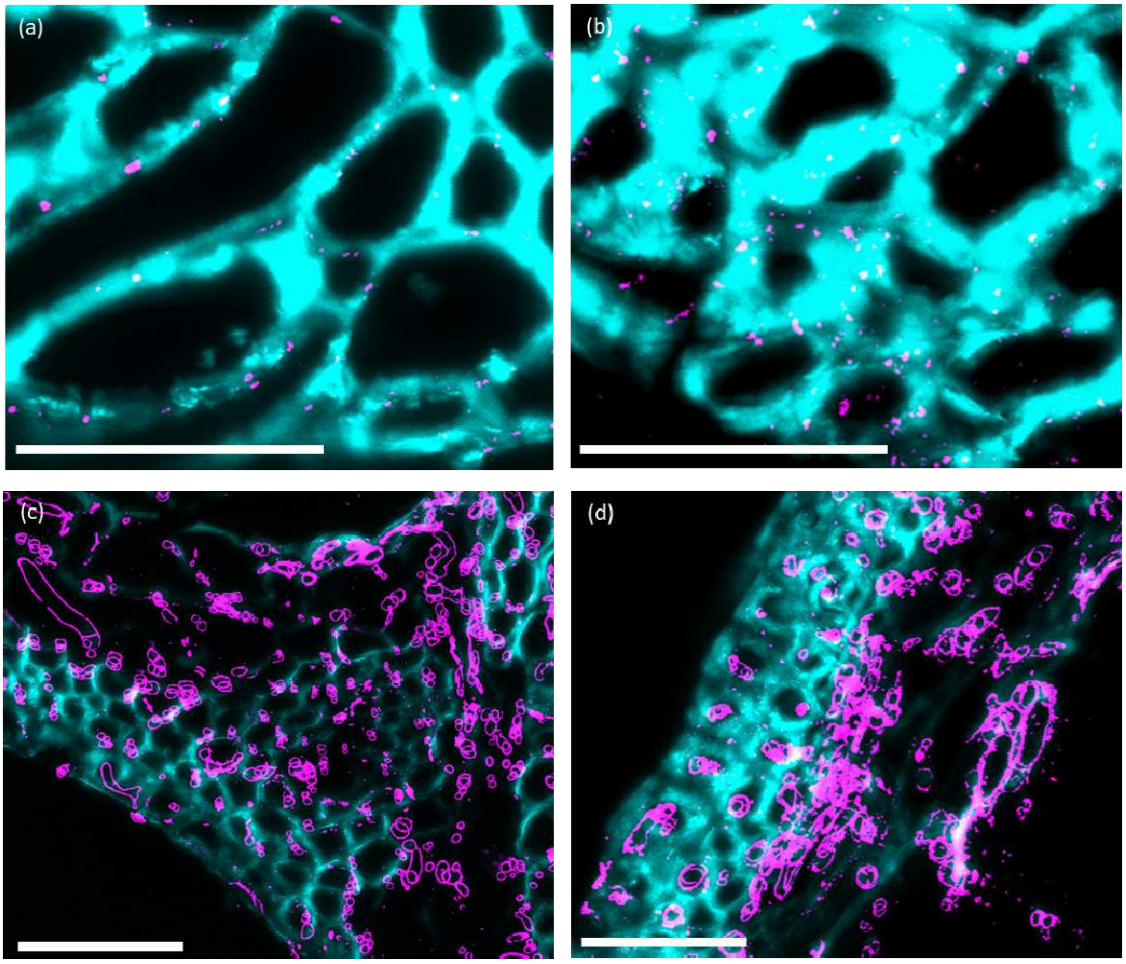

Fig. 8. Immunofluorescence detection of callose in rachis tissues. Magnified region of interest of the *Fg*-wheat interaction demonstrating callose deposits at the neck of plasmodesmata. (a) Control rachis, (b) DON-inoculated rachis, (c) PH-1 infected lemma at 5dpi, (d) *ΔTri5*-infected lemma at 5dpi. Sections were imaged by confocal microscopy with excitation-emission spectra for AlexFluor-488 488nm, 510nm-530nm and 405nm, 450nm-475nm for Calcofluor. Scale bars = 50µm. In panels (c) and (d) the Fusarium hyphae also react positively to the antibody due to □-1,3-glucans in the fungal cell wall.

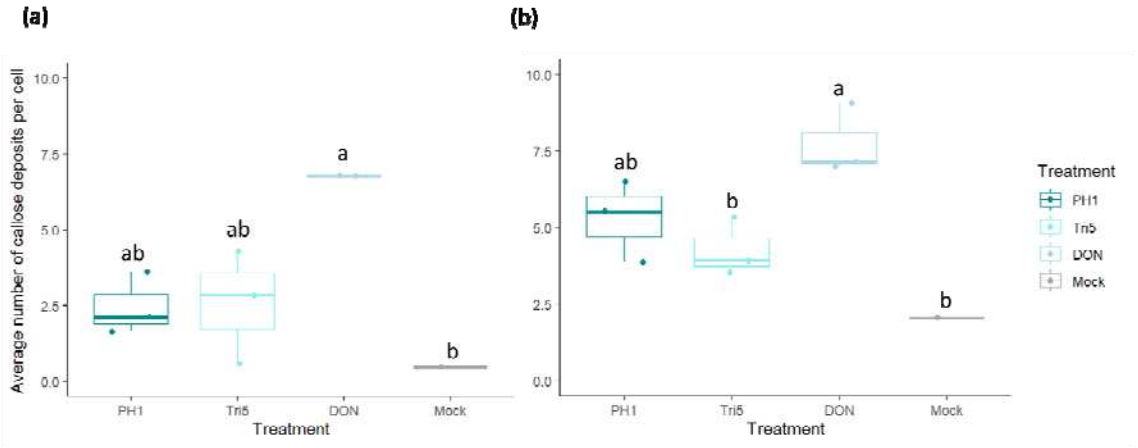

560 **Fig. 9. Quantification of immuno-labelled callose deposits in lemma and rachis tissues at 5dpi.** (a)
561 Lemma tissues at 5dpi, ANOVA = $p < 0.05$ (*), and (b) Rachis tissues at 5dpi, ANOVA = $p < 0.05$ (*).
562 Letters indicate significance between groups from Tukey Post-hoc analysis following one-way
563 ANOVA.

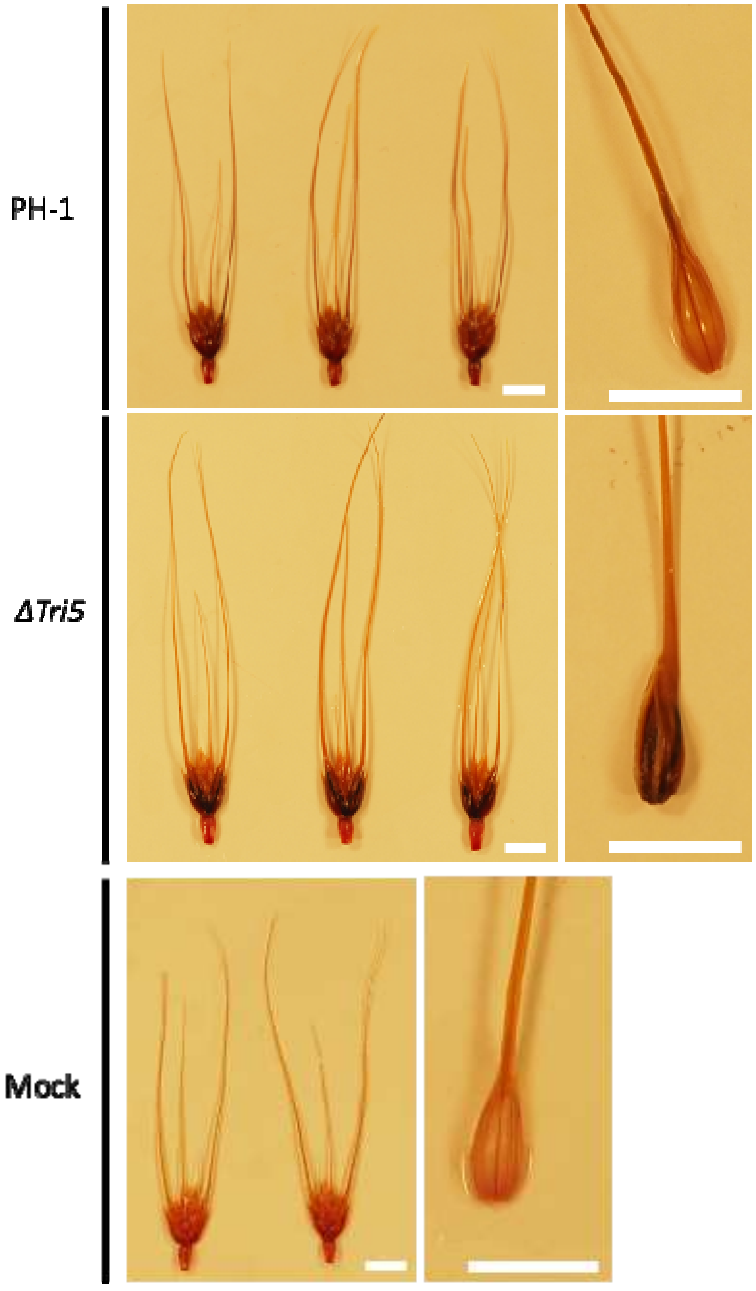

564

565 **Fig. 10. Phloroglucinol staining of infected spikelets for the detection of lignin.** Darker staining of
566 the tissues indicates a greater quantity of lignin. (a) PH-1 - infected spikelet, (b) *ΔTri5*-infected
567 spikelet, (c) Mock-inoculated spikelet. Spikelet component tissues: Lemma demonstrated an

increase in phloroglucinol staining component, shown to the left of each treatment, indicating an increase in lignin content. N.B. Point inoculations occur between the lemma and palea tissues. All spikelets were collected at 5dpi and are of the wheat cv. Apogee. Scale bar = 10mm.

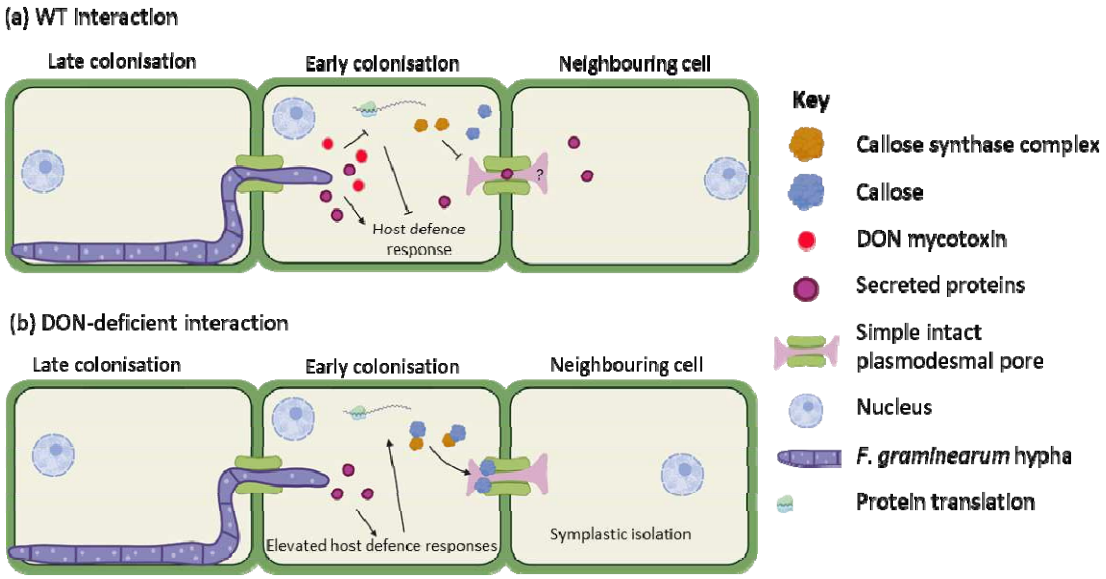

Fig. 11. Proposed working model for the role of DON in the *F. graminearum* – wheat interaction. (a) In the wild-type (WT) interaction, DON interferes with the wheat host defence response by inhibiting protein translation, reducing the ability of the host to deposit callose at plasmodesmata to restrict further infection. It is currently unknown how long the desmotubule remains functional, or in place. (b) In the absence of DON, *Fg*-secreted proteins are detected by the host and trigger host defence responses, including the symplastic isolation of neighbouring cells by the deposition of callose at plasmodesmata.

References

1. McMullen, M., Bergstrom, G., De Wolf, E., Dill-Macky, R., Hershman, D., Shaner, G. and Van Sanford, D. (2012). A unified effort to fight an enemy of wheat and barley: Fusarium head blight. *Plant Disease*, 96(12), 1712-1728. doi: 10.1094/PDIS-03-12-0291
2. McCormick, S. P., Stanley, A. M., Stover, N. A. and Alexander, N. J. (2011). Trichothecenes: from simple to complex mycotoxins. *Toxins*. 3(7), 802-814. doi: 10.3390/toxins3070802.
3. Brown, D. W., Dyer, R. B., McCormick, S. P., Kendra, D. F. and Plattner, R. D. (2004). Functional demarcation of the *Fusarium* core trichothecene gene cluster. *Fungal Genetics and Biology*. 41(4), 454-462. doi: 10.1016/j.fgb.2003.12.002.
4. McMullen, M., Jones, R. and Gallenburg, D. (1997). Scab of wheat and barley: a re-emerging disease of devastating impact. *Plant Disease*. 81(12), 1340 – 1348. doi: 10.1094/PDIS.1997.81.12.1340.

5. Vaughan, M., Backhouse, D. and Ponte, E. M. D. (2016). Climate change impacts on the ecology of *Fusarium graminearum* species complex and susceptibility of wheat to Fusarium head blight: a review. *World Mycotoxin Journal,* 9(5), 685–700. doi: 10.3920/WMJ2016.2053
6. Fan, J., Urban, M., Parker, J. E., Brewer, H. C., Kelly, S. L., Hammond-Kosack, K. E., Fraaije, B. A., Liu, X. and Cools, H. J. (2013). Characterization of the sterol 14α-demethylases of *Fusarium graminearum* identifies a novel genus-specific CYP51 function. New Phytologist 198(3), 821–835. doi: 10.1111/nph.12193.
7. Pritsch, C., Muehlbauer, G. J., Bushnell, W. R., Somers, D. A., and Vance, C. P. (2000). Fungal development and induction of defense response genes during early infection of wheat spikes by Fusarium graminearum. *Molecular Plant Microbe Interactions.* 13(2): 159-169. doi: 10.1094/MPMI.2000.13.2.159
8. Wanjiru, W. M., Zhensheng, K., and Buchenauer, H. (2002). Importance of cell wall degrading enzymes produced by *Fusarium graminearum* during infection of wheat heads. *European Journal of Plant Pathology*. 108: 803-810. doi: 10.1023/A:1020847216155.
9. Brown, N. A., Bass, C., Baldwin, T. K., Chen, H., Massot, F., Carion, P. W. C., Urban, M., van de Meene, A. M. L. and Hammond-Kosack, K. E. (2011). Characterisation of the *Fusarium*-wheat floral interaction. *Journal of Pathogens*. Article ID 626345. doi: 10.4061/2011/626345.scholar
10. Brown, N. A., Antoniw, J., Hammon-Kosack, K. E. (2012). The Predicted Secretome of the Plant Pathogenic Fungus *Fusarium graminearum*: A Refined Comparative Analysis. PLoS ONE, 7(4), e33731. doi:10.1371/journal.pone.0033731.
11. Guenther, J. C. and Trail, F. (2004). The development and differentiation of *Gibberella zeae* (anamorph: *Fusarium graminearum*) during colonization of wheat. *Mycologia*. 97(1), 229-237. doi: 10.1080/15572536.2006.11832856.
12. Parry, D.W., Jenkinson, P. and McLeod, L. (1995). Fusarium ear blight (scab) in small grain cereals—A review. *Plant Pathology*. 44, 207–238. doi: doi.org/10.1111/j.1365-3059.1995.tb02773.x.
13. Jansen, C., von Wettstein, D., Schäfer, W., Kogel, K-H., Felk, A., and Maier, F. J. (2005). Infection patterns in barley and wheat spikes inoculated with wild-type and trichodiene synthase gene disrupted *Fusarium graminearum*. *PNAS.* 102(46), 16892- 16897. Doi: 10.1073/pnas.0508467102.
14. Brown, N. A., Urban, M., van de Meene, A. M. L., and Hammond-Kosack, K. E. (2010). The infection biology of Fusarium graminearum definding the pathways of spikelet to spikelet colonisation in wheat ears. *Fungal Biology*. 114(7): 555-571. doi: 10.1016/j.funbio.2010.04.006.
15. Sager, R. E. and Lee, J. (2018). Plasmodesmata at a glance. *Journal of Cell Science.* 131(11), jcs209346. doi: 10.1242/jcs.209346.
16. Lee, J. and Lu, H. (2011). Plasmodesmata: the battleground against intruders. *Trends in Plant Science*. 16(4): 201-210. doi: 10.1016/j.tplants.2011.01.004.
17. Dilks, T., Halsey, K., De Vos, R. P., Hammond-Kosack, K. E. and Brown, N. A. (2019). Non-canonical fungal G-protein coupled receptors promote Fusarium head blight on wheat. *PLoS Pathogens*. 15(4): e1007666. doi: 10.1371/journal.ppat.1007666.
18. Hohn, T. M., McCormick, S. P. and Desjardins, A. E. (1993). Evidence for a gene cluster involving trichothecene-pathway biosynthetic genes in *Fusarium sporotrichioides*. *Current Genetics.* 24, 291-295. doi: 10.1007/bf00336778.

19. Proctor, R. H., Hohn, T. M. and McCormick, S. P. (1995). Reduced virulence of *Gibberella zeae* caused by disruption of a trichothecene toxin biosynthetic gene. *Molecular Plant-Microbe Interactions.* 8(4), 593-601. doi: 10.1094/mpmi-8-0593.
20. Cuzick, A., Urban, M. and Hammond-Kosack, K. (2008). *Fusarium graminearum* gene deletion mutants *map1* and *tri5* reveal similarities and differences in the pathogenicity requirements to cause disease on Arabidopsis and wheat floral tissue. *New Phytologist*. 177(4), 990-1000. doi: 10.1111/j.1469-8137.2007.02333.x
21. Hallen-Adams, H.E., Wenner, N., Kuldau, G. A. and Trail, F. (2011). Deoxynivalenol biosynthesis-realted gene expression during wheat kernel colonization by *Fusarium graminearum.* 101(9): 1091-1096. doi: 10.1094/PHYTO-01-11-0023.
22. Boenisch, M.J. and Schafer, W. (2011). *Fusarium graminearum* forms mycotoxin producing infection structures on wheat. *BMC Plant biology.* 11: 110. doi: 10.1186/1471-2229-11-110
23. Mesterházy, A. (1995). Types and components of resistance to *Fusarium* head blight of wheat. *Plant Breeding.* 114, 377-386. doi: 10.1111/j.1439-0523.1995.tb00816.x
24. Pestka, J. J. (2010). Deoxynivalenol: mechanisms of action, human exposure, and toxicological relevance. *Archives of Toxicology*. 84, 663-679. doi: 10.1007/s00204-010-0579-8.
25. Berthiller, F., Dall'Asta, C., Schuhmacher, R., Lemmens, M., Adam, G. and Krska, R. (2005). Masked mycotoxins: determination of a deoxynivalenol glucoside in artificially and naturally contaminated wheat by liquid chromatography–tandem mass spectrometry. *Journal of Agricultural and Food Chemistry.* 53(9), 3421-3425. doi: 10.1021/jf047798g.
26. Wu, S., Kumar, R., Iswanto, A. B. B, and Kim, J. (2018). Callose balancing at plasmodesmata. *Journal of Experimental Botany*. 69(22), 5325-5339. doi: 10.1093/jxb/ery317.
27. Ellinger, D., Naumann, M., Falter, C., Zwikowics, C., Jamrow, T., Manisseri, C., Somerville, S. C. and Voigt, C. A. (2013). Elevated early callose deposition results in complete penetration resistance to powdery mildew in Arabidopsis. 161(3): 1433-1444. doi: 10.1104/pp.112.211011
28. Kashyap, A., Planas-Marquès, M., Capellades, M., Valls, M. and Coll, N. S. (2021). Blocking intruders: inducible physico-chemical barriers against plant vascular wilt pathogens. *Journal of Experimental Botany.* 72(2): 184-198. doi: 10.1093/jxb/eraa444.
29. Wang, Z., Yang, B., Zheng, W., Wang, L., Cai, X., Yang, J., Song, R., Yang, S., Wang, Y., Xiao, J., Liu, H., Wang, Y., Wang, X., Yuanchao, W. (2022). Recognition of glycoside hydrolase 12 proteins by the immune receptor RXEG1 confers *Fusarium* head blight resistance in wheat. *Plant Biotechnology Journal*. 21(4): 769-781. doi: 10.1111/pbi.13995.
30. Evans, C. K., Xie, W., Dill-Macky, R. and Mirocha, C. J. (2000). Biosynthesis of deoxynivalenol in spikelets of Barley inoculated with macronidia of *Fusarium graminearum.* 84(6): 654-660. doi: 10.1094/PDIS.2000.84.6.654.
31. Chen, Y., Kistler, H. C., and Ma, Z. (2019). *Fusarium graminearum* trichothecene mycotoxins: biosynthesis, regulation, and management. *Annual Review Phytopathology.* 57, 15-39. doi: 10.1146/annurev-phyto-082718-100318.
32. Ilgen, P., Hadeler, B., Maier, F. J. and Schäfer, W. (2009). Developing Kernel and Rachis Node Induce the Trichothecene Pathway *of Fusarium graminearum* During Wheat Head Infection. *Molecular Plan-Microbe Interactions*, 22(8), 899-908. doi: 10.1094 / MPMI -22-8-0899.

33. Zhang, X-W., Jia, L-J., Zhang, Y., Li, X., Zhang, D. and Tang, W-H. (2012). In planta stage-specific fungal gene profiling elucidates the molecular strategies of *Fusarium graminearum* growing inside wheat coleoptiles. 24(12). 5159-5176. doi: 10.1105/tpc.112.105957.
34. Gardiner, D. M., Kazan, K. and Manners, J. M. (2009). Nutrient profiling reveals potent inducers of trichothecene biosynthesis in *Fusarium graminearum*. *Fungal Genetics and Biology.* 46, 604–613. doi: 10.1016/j.fgb.2009.04.004.
35. Gardiner, D. M., Osbourne, S., Kazan, K. and Manners, J. M. (2009). Low pH regulates the productions of deoxynivalenol by *Fusarium graminearum*. 155(9), 3149-3156. doi: 10.1099/mic.0.029546-0.
36. Sakulkoo, W., Oses-Ruiz M., Garcia E. O., Soanes, D. M., Littlejohn, G. R., Hacker, C., Correia, A., Valent, B. and Talbot, N. J. (2018). A single fingal MAP kinase controls plant cell-to-cell invasion by the rice blast fungus. *Science*. 359(6382), 1399-1403. doi: 10.1126/science.aaq0892.
37. Fernandez, J. and Orth, K. (2018). Rise of a cereal killer: The biology of *Magnaporthe oryzae* biotrophic growth. *Trends in Microbiology*. 26(7), 582-597. doi: 10.1016/j.tim.2017.12.007.
38. Wilson, R. A. and Talbot, N. J. (2009). Under pressure: investigating the biology of plant infection by *Magnaporthe oryzae*. *Nature Reviews Microbiology,* 7, 185-195. doi: 10.1038/nrmicro2032.
39. Darino, M, Urban, M, Kaur, N, Machado-Wood, A, Grimwade-Mann, M, Smith, D, Beacham, A and Hammond-Kosack, K. (2023). Identification and functional characterisation of a locus for target site integration in *Fusarium graminearum. bioRxiv.* doi: 10.1101/2023.08.20.553861.
40. Lemmens, M., Scholz, U., Berthiller, F., Dall'Asta, C., Koutnik, A., Schuhmacher, R., Adam, G., Buerstmayr, H., Mesterházy, Á., Krska, R. and Ruckenbauer, P. (2005). The ability to detoxify the mycotoxin deoxynivalenol colocalizes with a major quantitative trait locus for Fusarium Head Blight resistance in wheat. *Molecular Plant Microbe Interactions*. 18(12), 1318-1324. doi: 10.1094/MPMI-18-131.
41. Van Der Plank, J. E. (1963). Plant diseases: epidemics and control. Academic Press, New York.
42. Mendiburu, F. and Yaseen, M. (2020). agricolae: statistical procedures for agricultural research. R package version 1.4.0.
43. Wickham, H. (2016). *ggplot2: Elegant Graphics for Data Analysis*. Springer-Verlag, New York.
44. Amsbury, S. and Benitez-Alfonso, Y. (2022). Chapter 10: Immunofluorescence detection of callose in plant tissue sections. In: Benitez-Alfonso, Y. and Heinlein, M. (eds.): *Plasmodesmata: Methods and Protocols*, Methods in Molecular Biology, vol. 2457. doi: 10.1007/978-1-0716-2132-5_10.
45. Mitra, P. P. and Loque. D. (2014). Histochemical staining of *Arabidopsis thaliana* secondary cell wall elements. *Journal of Visualized Experiments.* 87: 51381. doi: 10.3791/51381.
46. Cavinder, B., Sikhakolli, U., Fellows, K. M. and Trail, F. (2012). Sexual development and ascospore discharge in Fusarium graminearum. *Journal Visualized Experiments.* 61, 3895. doi: 10.3791/3895.

Acknowledgements

The authors would like to thank the CHAP organisation at Rothamsted for access to their Lemnagrid image analysis software. Special thanks are given to Hannah Walpole and Kirstie Halsey from

Rothamsted Research Bioimaging department for continued training, advice and expertise. Martin Urban and Kim Hammond-Kosack are supported by the Biotechnology and Biological Sciences Research Council (BBSRC) Institute Strategic Programme (ISP) Grant, Delivering Sustainable Wheat (BB/X011003/1) and the BBSRC grants (BB/X012131/1 and BB/W007134/1). Victoria Armer is supported by the BBSRC-funded South West Biosciences Doctoral Training Partnership (BB/T008741/1).

Author contributions

VA conducted the experiments and wrote the manuscript, MU generated the Fusarium graminearum mutant, TA provided oversight and training for image analysis, MJD and KHK provided project oversight, experimental design and manuscript revisions.

Additional Information

The authors declare no financial or non-financial competing interests. The research data supporting this publication are provided within this paper. Requests for materials relating to this paper should be made to Kim Hammond-Kosack (kim.hammond-kosack@rothamsted.ac.uk) at Rothamsted Research.